R. & M. No. 3240

MINISTRY OF AVIATION

AERONAUTICAL RESEARCH COUNCIL
REPORTS AND MEMORANDA

The Flow past a Pitot Tube at Low Reynolds Numbers

Part I.—The Numerical Solution of the Navier-Stokes Equations for Steady Viscous Axi-symmetric Flow

Part II.—The Effects of Viscosity and Orifice Size on a Pitot Tube at Low Reynolds Numbers

By W. G. S. Lester
Department of Engineering Science, University of Oxford

LONDON: HER MAJESTY'S STATIONERY OFFICE
1961
PRICE: 9*s*. 6*d*. NET

The Flow past a Pitot Tube at Low Reynolds Numbers

By W. G. S. Lester

Department of Engineering Science, University of Oxford

*Reports and Memoranda No. 3240**

July, 1960

Part I.—The Numerical Solution of the Navier-Stokes Equations for Steady Viscous Axi-symmetric Flow

Summary. In this Report numerical methods used to solve the Navier-Stokes equations for steady viscous two-dimensional flow are extended to include the case of axial symmetry. The equations and their finite difference approximations are derived working in cylindrical polar co-ordinates with the Stokes' stream function and the vorticity as variables. A new method of dealing with the boundary conditions is given.

1.1. *Introduction.* The problem of solving the Navier-Stokes equations for the flow of a viscous, incompressible fluid past an obstacle is a matter of considerable complexity. The theory of non-linear partial differential equations is as yet insufficiently developed to provide a general analytical method of solution. A numerical approach is the only one that has so far been productive. In two dimensions numerical methods have been successfully developed and applied to specific problems, the majority of the earlier work having been done by Thom[1].

The main difficulties arise from the non-linearity of the equations and under certain circumstances it has been possible to simplify them to some extent and make them tractable by analytic means. The non-linear terms in the equations are the inertia terms and if these are neglected after the manner of Stokes, or only partially taken into account as in the Oseen theory, analytical methods can be used to study the very slow motion of a viscous fluid. These solutions are only valid for an extremely low Reynolds number and when the viscous and inertial forces become comparable in magnitude the theory is no longer applicable. Even in the simplest cases the analysis is difficult and can only be used on a few types of body profile. When a slightly viscous fluid flows past a body the viscous and inertia forces are only comparable in a very thin layer of fluid near to the body surface and the methods of Prandtl's boundary-layer theory may be used. Numerical and analytical solutions have been obtained for many profiles; the reader is referred to Schlichting[2] for a survey of the theory. There remains a wide range where neither the slow motion theory or boundary-layer theory can be applied and the full Navier-Stokes equations must be solved. It is primarily with this region that we are concerned.

In the axi-symmetric case the full equations have proved intractable analytically and only a few exact solutions of them are known, most of which have little physical relevance. Numerical methods have attracted little attention, mainly due to the difficulty of solving the rather unwieldy finite

* Previously issued as O.U.E.L. No. 136—A.R.C. 22,070.

difference equations whose non-linearity has made attempts at solution extremely long and tedious. Even in the solution for slow flows, using the Stokes' approximation, by numerical methods the labour required is almost prohibitive and the inclusion of the non-linear terms so complicates the problem as to make it impracticable for solution by hand. However, the growing use of electronic computors removes much of the difficulty and affords encouragement for the development of a satisfactory routine method. The machine time used can be quite high even with a relatively straightforward problem. The success of a solution may well depend to a large extent on the choice of the initial starting values; to build up a solution with all function values initially zero may seem the best procedure but has the disadvantage of taking so much machine time. On the other hand, an unfortunate choice can easily lead to divergence in the numerical process employed. It should be emphasised that this divergence arises from the numerical method and has no connection with hydrodynamic stability since steady flow is postulated. Divergence can usually be combated when working by hand but can be difficult to deal with on a computer, the usual technique being either to reduce the mesh size or employ only a partial movement in function values at mesh points.

The first attempt to obtain a numerical solution was made by Thom[3] who examined the slow motion of a viscous fluid through an abrupt expansion in a circular pipe, working in cylindrical polar co-ordinates and solving the Stokes' equations. The only work valid at a finite Reynolds number appears to be that of Jenson[4] who has produced solutions for the flow past a sphere placed on the axis of a circular pipe at Reynolds numbers up to forty (based on the sphere diameter). The co-ordinate system used was spherical polars.

Some of the methods applicable in two dimensions will now be extended to the case of axially symmetric flows using cylindrical co-ordinates. The working variables are the Stokes' stream function ψ and the vorticity ζ. In two dimensions, this two-field related system of variables, first introduced by Thom[1], has been shown by Fox[5] to have a faster rate of convergence than if the single variable ψ had been used. It is to be expected that a similar result will hold for the axially symmetric case. An accurate formula to relate ζ and ψ at a solid boundary, analogous to Woods' formula in two dimensions (Ref. 6), is derived. This formula has been found to be quite satisfactory in the problems so far considered and gives a reasonable rate of convergence. It has unfortunately not yet proved possible to derive an easily applied convergence criterion as for the two-dimensional flow (Ref. 7), but in practice it seems that the two-dimensional test does give some indication as to when divergence can be expected.

As an example of the method and the technique used, the effects of viscosity on a pitot tube at a low Reynolds number have been investigated in some detail in Part II.

1.2. *The Axially Symmetric Form of the Navier-Stokes Equations.* A brief derivation of the axially symmetric form of the equations in cylindrical co-ordinates is now included.
In terms of Stokes' stream function the velocity components may be written

$$q_z = -\frac{1}{r}\frac{\partial \psi}{\partial r}; \; q_r = \frac{1}{r}\frac{\partial \psi}{\partial z}; \; q_\phi = 0$$

and the vorticity components

$$(\text{curl } q)_z = 0; \quad (\text{curl } q)_r = 0; \quad (\text{curl } q)_\phi = \frac{\partial q_r}{\partial z} - \frac{\partial q_z}{\partial r} = \zeta .$$

If $\mathbf{i}_z$, $\mathbf{i}_\phi$, and $\mathbf{i}_r$ are unit vectors in the meridian plane and perpendicular to that plane,

$$\mathbf{q} = q_z\mathbf{i}_z + q_r\mathbf{i}_r, \text{ and } \boldsymbol{\zeta} = \zeta\mathbf{i}_\phi .$$

In vector form the Navier-Stokes equations are

$$\frac{\partial \boldsymbol{\zeta}}{\partial t} - \nabla_A(\mathbf{q}_A\boldsymbol{\zeta}) = -\nu\nabla_A(\nabla_A\boldsymbol{\zeta}). \tag{1}$$

Now

$$-\nabla_A(\mathbf{q}_A\boldsymbol{\zeta}) = \left\{\frac{\partial(q_z\zeta)}{\partial z} + \frac{\partial(q_r\zeta)}{\partial r}\right\}\mathbf{i}_\phi \tag{2}$$

$$\nabla_A(\nabla_A\boldsymbol{\zeta}) = -\left\{\frac{\partial}{\partial z}\left(\frac{1}{r}\frac{\partial(r\zeta)}{\partial z}\right) + \frac{\partial}{\partial r}\left(\frac{1}{r}\frac{\partial(r\zeta)}{\partial r}\right)\right\}\mathbf{i}_\phi \tag{3}$$

$$\zeta = \frac{\partial q_r}{\partial z} - \frac{\partial q_z}{\partial r} = \frac{1}{r}\left\{\frac{\partial^2\psi}{\partial z^2} + \frac{\partial^2\psi}{\partial r^2} - \frac{1}{r}\frac{\partial\psi}{\partial r}\right\} = \frac{1}{r}E^2\psi \tag{4}$$

where

$$E^2 \equiv \frac{\partial^2}{\partial z^2} + \frac{\partial^2}{\partial r^2} - \frac{1}{r}\frac{\partial}{\partial r}.$$

The equation of continuity is

$$\frac{\partial(q_z r)}{\partial z} + \frac{\partial(q_r r)}{\partial r} = 0. \tag{5}$$

From (2) and (5),

$$-\nabla_A(\mathbf{q}_A\boldsymbol{\zeta}) = r\left\{q_z\frac{\partial}{\partial z}\left(\frac{\zeta}{r}\right) + q_r\frac{\partial}{\partial r}\left(\frac{\zeta}{r}\right)\right\}\mathbf{i}_\phi.$$

From (4) and (3),

$$\nabla_A(\nabla_A\boldsymbol{\zeta}) = -\frac{E^4\psi}{r}\mathbf{i}_\phi.$$

Substituting in (1)

$$r\frac{\partial\zeta}{\partial t} + r\frac{\partial(\psi,\ \zeta/r)}{\partial(z,\ r)} - \nu E^4\psi = 0.$$

Assuming steady motion

$$E^4\psi - \frac{r}{\nu}\frac{\partial(\psi,\ \zeta/r)}{\partial(z,\ r)} = 0. \tag{6}$$

Equations (4) and (6) will be considered in the form

$$\Delta^2\psi = r\zeta + \frac{1}{r}\frac{\partial\psi}{\partial r} \tag{7}$$

$$\Delta^2\zeta = \frac{1}{r}\left(\frac{\zeta}{r} - \frac{\partial\zeta}{\partial r}\right) + \frac{1}{\nu r}\left\{\frac{\partial\psi}{\partial z}\frac{\partial\zeta}{\partial r} - \frac{\partial\psi}{\partial r}\frac{\partial\zeta}{\partial z}\right\} - \frac{\zeta}{\nu r^2}\frac{\partial\psi}{\partial z} \tag{8}$$

where

$$\Delta^2 \equiv \frac{\partial^2}{\partial r^2} + \frac{\partial^2}{\partial z^2}.$$

It is interesting to note that many of the known exact solutions of the axially symmetric equations can easily be obtained from Equations (7) and (8) by assuming that ψ is of the form $Az^m r^n$, where A is a constant. The solutions obtained by substitution and equating the coefficients to zero are

$$\psi = A;\ Ar^2;\ Ar^4;\ Az;\ Azr^2;\ Az^2r^2$$

and the particular case

$$\psi = 2\nu r^2/z\,.$$

Working in spherical polar co-ordinates the solution $\psi = 2\nu r^2/z$ (the well-known round laminar jet) has been obtained by Squire[8], and the solution $\psi = Az^2r^2$ given by Agrawal[9].

1.3. *Boundary Conditions.* The usual conditions to be satisfied at a solid boundary are that no slipping should occur there and that there should be no flux across the boundary.

In terms of the stream function ψ these can be expressed as

$$\psi = \text{constant};\quad \frac{\partial\psi}{\partial r} = 0;\quad \frac{\partial\psi}{\partial z} = 0\,. \tag{9}$$

1.4. *The Determination of Pressure Differences.* The axially symmetric equations are considered in the form

$$F_r - \frac{1}{\rho}\frac{\partial p}{\partial r} = \frac{\partial q_r}{\partial t} + q_r\frac{\partial q_r}{\partial r} + q_z\frac{\partial q_r}{\partial z} - \nu\left\{\frac{\partial^2 q_r}{\partial r^2} + \frac{1}{r}\frac{\partial q_r}{\partial r} + \frac{\partial^2 q_r}{\partial z^2}\right\}$$

$$F_z - \frac{1}{\rho}\frac{\partial p}{\partial z} = \frac{\partial q_z}{\partial t} + q_r\frac{\partial q_z}{\partial r} + q_z\frac{\partial q_z}{\partial z} - \nu\left\{\frac{\partial^2 q_z}{\partial r^2} + \frac{1}{r}\frac{\partial q_z}{\partial r} + \frac{\partial^2 q_z}{\partial z^2}\right\}$$

together with the equation of continuity,

$$\frac{\partial q_r}{\partial r} + \frac{\partial q_z}{\partial z} = -\frac{q_r}{r}\,.$$

Deleting the time derivatives and integrating along a path AB in the fluid we have

$$\int_A^B \{F_r dr + F_z dz\} - \frac{1}{\rho}(p_B - p_A) = \int_A^B \left(q_r\frac{\partial q_r}{\partial r} + q_z\frac{\partial q_r}{\partial z}\right) dr +$$

$$+ \int_A^B \left(q_r\frac{\partial q_z}{\partial r} + q_z\frac{\partial q_z}{\partial z}\right) dz - \nu\int_A^B \{\nabla^2 q_r dr + \nabla^2 q_z dz\}\,.$$

Now,

$$\int_A^B \left\{\left(q_r\frac{\partial q_r}{\partial r} + q_z\frac{\partial q_r}{\partial z}\right) dr + \left(q_r\frac{\partial q_z}{\partial r} + q_z\frac{\partial q_z}{\partial z}\right) dz\right\} = \int_A^B \{q_r dq_r + q_z dq_z - q_r\zeta dz + q_z\zeta dr\}$$

also

$$\int_A^B \{\nabla^2 q_r dr + \nabla^2 q_z dz\} = \int_A^B \left\{\left(\frac{\partial\zeta}{\partial z} + \frac{q_r}{r^2}\right) dr - \left(\frac{\partial\zeta}{\partial r} + \frac{\zeta}{r}\right) dz\right\}.$$

Hence

$$\int_A^B \{F_r dr + F_z dz\} - \frac{1}{\rho}(p_B - p_A) = \frac{q_B^2}{2} - \frac{q_A^2}{2} - \int_A^B \left\{\frac{\zeta}{r}\frac{\partial\psi}{\partial z} dz + \frac{\zeta}{r}\frac{\partial\psi}{\partial r} dr\right\} -$$

$$- \nu\int_A^B \left(\left\{\frac{\partial\zeta}{\partial z} + \frac{1}{r^3}\frac{\partial\psi}{\partial z}\right\} dr - \left\{\frac{\partial\zeta}{\partial r} + \frac{\zeta}{r}\right\} dz\right). \tag{10}$$

This equation enables the pressure difference between any two points A and B in the fluid to be determined by integration along a path connecting them.

1.5. *The Non-Dimensional Form of the Equations.* It is frequently convenient to work with the equations in a non-dimensional form. If a dash is used to denote a non-dimensional quantity,

$$r = Lr', \quad z = Lz', \quad q = Uq', \quad F = \frac{U}{L}F', \quad p = \tfrac{1}{2}\rho U^2 p', \quad \psi = UL\psi' \text{ and } \zeta = \frac{U}{L}\zeta',$$

where U is a representative velocity and L a representative length.

Substituting these expressions in Equations (4) and (6) of Section 1.2:

$$E'^2\psi' = r'\zeta' \tag{11}$$

$$r'E'^2(r'\zeta') = Re\left\{\frac{\partial\psi'}{\partial z'}\frac{\partial\zeta'}{\partial r'} - \frac{\partial\psi'}{\partial r'}\frac{\partial\zeta'}{\partial z'} - \frac{\zeta'}{r'}\frac{\partial\psi'}{\partial z'}\right\} \tag{12}$$

where Re is a Reynolds number UL/ν, and

$$E'^2 \equiv \frac{\partial^2}{\partial z'^2} + \frac{\partial^2}{\partial r'^2} - \frac{1}{r'}\frac{\partial}{\partial r'}.$$

The equation to determine the pressure difference between two points becomes

$$2\int_{A'}^{B'}(F_r'dr' + F_z'dz') - (p_B' - p_A') = q_B'^2 - q_A'^2 - 2\int_{A'}^{B'}\left\{\frac{\zeta'}{r'}\frac{\partial\psi'}{\partial z'}dz' + \frac{\zeta'}{r'}\frac{\partial\psi'}{\partial r'}dr'\right\} -$$

$$-\frac{2}{Re}\int_{A'}^{B'}\left\{\left(\frac{\partial\zeta'}{\partial z'} + \frac{1}{r'^3}\frac{\partial\psi'}{\partial z'}\right)dr' - \left(\frac{\partial\zeta'}{\partial r'} + \frac{\zeta'}{r'}\right)dz'\right\} \tag{13}$$

where A' and B' are the points corresponding to A and B in the non-dimensional form.

1.6. *The Numerical Solution of the Equations.* The technique used in the numerical solution of the axially symmetric equations is similar to that used by Thom in two-dimensional problems. The continuous field of flow is replaced by a rectangular mesh and at the mesh points assumed values of ψ and ζ are placed. These values of ψ and ζ are then recalculated alternately by means of finite difference approximations to the Equations (7) and (8), with assumed values of ζ on the solid boundaries. From the new configurations of ψ and ζ in the neighbourhood of the boundary new boundary values of ζ have to be calculated. The whole process is then repeated until the values of ψ and ζ are repeated everywhere to the required degree of accuracy.

1.7. *Finite Difference Approximations to the Navier-Stokes Equations.* The simplest finite difference approximations to the Equations (7) and (8) of Section 1.2 are based on two point differentiation. With a diamond (*i.e.*, the mesh is orientated as shown in Fig. 1), the approximations are given by

$$\psi_O = \psi_m - \frac{n}{8r}(D-B) - \frac{rn^2}{4}\zeta_0 \tag{14}$$

$$\zeta_0\left\{1 + \frac{n^2}{4r^2} - \frac{n}{8r^2\nu}(A-C)\right\} = \zeta_m + \frac{n}{8r}(d-b) - \frac{1}{16r\nu}\{(A-C)(d-b) - (D-B)(a-c)\}, \tag{15}$$

where capital letters are used to denote the values of ψ and small letters values of ζ at the corresponding mesh points as shown in Fig. 1. The suffix 'm' indicates that the mean of the function values at the four points A, B, C, and D is taken.

If a square mesh is considered, as in Fig. 2, then the finite difference approximations are given, with a similar notation to that for a diamond, by

$$\psi_0 = \psi_m - \frac{\mathrm{n}}{8\mathrm{r}}(\mathrm{A}+\mathrm{D}-\mathrm{B}-\mathrm{C}) - \frac{\mathrm{rn}^2}{2}\zeta_0 \tag{16}$$

$$\zeta_0\left\{1+\frac{n^2}{2r^2}-\frac{n}{8r^2\nu}(A+B-C-D)\right\} = \zeta_m + \frac{n}{8r}(a+d-b-c) - \\ - \frac{1}{16r\nu}\{(B-D)(a-c)-(A-C)(b-d)\}. \tag{17}$$

Alternatively, the first derivatives occurring in Equations (7) and (8) can be calculated using the five point differentiation formula. In view of the wider spread of points required it is difficult to say whether the accuracy of the solution is improved by this, it is, in any case, inadvisable to use any but the simplest approximations in the early stages of a calculation until a reasonably settled solution has been obtained, refinements can then be made in an attempt to improve the accuracy.

Owing to the non-linearity of the equations simple formulae analogous to the 'twelve' and 'twenty' (Ref. 10) used in two dimensions cannot be derived.

1.8. *Treatment of the Boundary Conditions.* For convenience the axially symmetric equations are considered in the form

$$E^2\psi = \zeta^* \tag{18}$$

$$E^2\zeta^* = f(r, z) \tag{19}$$

where

$$E^2 \equiv \frac{\partial^2}{\partial z^2} + \frac{\partial^2}{\partial r^2} - \frac{1}{r}\frac{\partial}{\partial r};$$

$$\zeta^* = r\zeta;\ f(r, z) = \frac{r}{\nu}\frac{\partial(\psi, \zeta/r)}{\partial(z, r)}$$

and r and z are cylindrical polar co-ordinates.

At a solid boundary ψ is known and is constant, but the values of ζ are usually unknown and must be calculated from the flow pattern in the neighbouring area of the boundary. In solving the finite difference approximations to the Equations (18) and (19) the procedure is to recalculate the values of ψ and ζ for certain assumed values of ζ at the boundary. Boundary values of ζ are then recalculated from the new values of ψ and ζ in the neighbouring flow.

The usual conditions appertaining to a viscous flow problem are

$$\psi = \text{constant} = \psi_0;\ \frac{\partial\psi}{\partial r} = 0;\ \frac{\partial\psi}{\partial z} = 0 \tag{20}$$

on a solid boundary.

In order to derive a finite difference equation for obtaining ζ on a solid boundary subject to the conditions given in Equation (20), the configuration shown in Fig. 3 is considered. Suppose the r and z axes are rotated through an angle θ so that the new Z axis is parallel to the tangent to ψ = constant at 0, and the new R axis is parallel to the normal at 0, then

$$\begin{aligned} Z &= z\cos\theta + r\sin\theta \\ R &= r\cos\theta - z\sin\theta \\ r &= Z\sin\theta + R\cos\theta \end{aligned} \tag{21}$$

and

$$\frac{\partial}{\partial r} \equiv \cos\theta\frac{\partial}{\partial R} + \sin\theta\frac{\partial}{\partial Z} \tag{22}$$

$$\frac{\partial}{\partial z} \equiv -\sin\theta\frac{\partial}{\partial R} + \cos\theta\frac{\partial}{\partial Z}. \tag{23}$$

Equations (18) and (19) transform to become

$$\frac{\partial^2\psi}{\partial R^2} + \frac{\partial^2\psi}{\partial Z^2} - \frac{1}{(Z\sin\theta + R\cos\theta)}\left\{\cos\theta\frac{\partial\psi}{\partial R} + \sin\theta\frac{\partial\psi}{\partial Z}\right\} = \zeta^* \tag{24}$$

$$\frac{\partial^2\zeta^*}{\partial R^2} + \frac{\partial^2\zeta^*}{\partial Z^2} - \frac{1}{(Z\sin\theta + R\cos\theta)}\left\{\cos\theta\frac{\partial\zeta^*}{\partial R} + \sin\theta\frac{\partial\zeta^*}{\partial Z}\right\} = f', \tag{25}$$

where f' is used to denote $f(r, z)$ in the transformed plane. On the boundary:

$$\frac{\partial\psi}{\partial R} = 0; \frac{\partial\psi}{\partial Z} = 0; \psi = \psi_0. \tag{26}$$

Considering a point 2 on the normal to ψ = constant at a distance h from 0 in the direction of R increasing, Taylor's theorem gives

$$\psi_2 = \psi_0 + h\frac{\partial\psi_0}{\partial R} + \frac{h^2}{2}\frac{\partial^2\psi_0}{\partial R^2} + \frac{h^3}{6}\frac{\partial^3\psi_0}{\partial R^3} + \frac{h^4}{24}\frac{\partial^4\psi_0}{\partial R^4} + O(h^5). \tag{27}$$

Differentiating Equation (24) and evaluating at the point 0 making use of the boundary conditions (26), the fact that all derivatives with respect to Z are zero and $\frac{\partial^3\psi_0}{\partial R\partial Z^2} = 0$, the following relations can be obtained:

$$\frac{\partial^2\psi_0}{\partial R^2} = \zeta_0^* \tag{28}$$

$$\frac{\partial^3\psi_0}{\partial R^3} = \frac{\partial\zeta_0^*}{\partial R} + \frac{\cos\theta}{(Z_0\sin\theta + R_0\cos\theta)}\zeta_0^* \tag{29}$$

$$\frac{\partial^4\psi_0}{\partial R^4} + \frac{\partial^4\psi_0}{\partial R^2\partial Z^2} + \frac{\cos^2\theta\,.\,\zeta_0^*}{(Z_0\sin\theta + R_0\cos\theta)} - \frac{\cos\theta}{(Z_0\sin\theta + R_0\cos\theta)}\cdot\frac{\partial\zeta_0^*}{\partial R} - \\ - \frac{\sin\theta}{(Z_0\sin\theta + R_0\cos\theta)}\cdot\frac{\partial^3\psi_0}{\partial R^2\partial Z} = \frac{\partial^2\zeta_0^*}{\partial R^2} \tag{30}$$

$$\frac{\partial^3\psi_0}{\partial R^2\partial Z} = \frac{\partial\zeta_0^*}{\partial Z} \tag{31}$$

$$\frac{\partial^4\psi_0}{\partial R^2\partial Z^2} = \frac{\partial^2\zeta_0^*}{\partial Z^2}. \tag{32}$$

From (30), (31) and (32), making use of (25),

$$\frac{\partial^4\psi_0}{\partial R^4} = 2\frac{\partial^2\zeta_0^*}{\partial R^2} - f_0' - \frac{\cos^2\theta\,.\,\zeta_0^*}{(Z_0\sin\theta + R_0\cos\theta)^2}. \tag{33}$$

Substituting from (28), (29) and (33) in (27),

$$\psi_2 = \psi_0 + \frac{h^2}{2}\zeta_0^* + \frac{h^3}{6}\left\{\frac{\partial\zeta_0^*}{\partial R} + \frac{\zeta_0^*\cos\theta}{Z_0\sin\theta + R_0\cos\theta}\right\}$$
$$+ \frac{h^4}{24}\left\{2\frac{\partial^2\zeta_0^*}{\partial R^2} - \frac{\cos^2\theta\,.\,\zeta_0^*}{(Z_0\sin\theta + R_0\cos\theta)^2} - f_0'\right\} + O(h^5). \tag{34}$$

Also, by Taylor's theorem,

$$\zeta_2^* = \zeta_0^* + h\frac{\partial\zeta_0^*}{\partial R} + \frac{h^2}{2}\frac{\partial^2\zeta_0^*}{\partial R^2} + O(h^3) \tag{35}$$

Eliminating $\partial\zeta_0^*/\partial R$ from (34) and (35) and rearranging, the terms in $\partial^2\zeta_0^*/\partial R^2$ cancel out and

$$\zeta_0^* = \frac{\left\{\frac{6}{h^2}(\psi_2-\psi_0) - \zeta_2^* + \frac{h^4}{4}f_0'\right\}}{\left\{2 + \frac{h\cos\theta}{(Z_0\sin\theta + R_0\cos\theta)} - \frac{h^2\cos^2\theta}{4(Z_0\sin\theta + R_0\cos\theta)^2}\right\}}.$$

Transferring to the original (r, z) co-ordinates this becomes

$$\zeta_0^* = \frac{\left\{\frac{6}{h_2}(\psi_2-\psi_0) - \zeta_2^* + \frac{h^4}{4}f_0\right\}}{\left\{2 + \frac{h\cos\theta}{r_0} - \frac{h^2\cos^2\theta}{4r_0^2}\right\}}. \tag{36}$$

In the axially symmetric form of the Navier-Stokes equations

$$E^2\psi = r\zeta$$

$$E^2(r\zeta) = \frac{r}{\nu}\frac{\partial(\psi, \zeta/r)}{\partial(z, r)} = f(r, z).$$

At the boundary

$$\frac{\partial\psi_0}{\partial r} = 0; \frac{\partial\psi_0}{\partial z} = 0$$

and so f_0 is zero.

The correct form of finite difference equation for use at the boundary is given by replacing ζ^* in Equation (36) by $r\zeta$, and f_0 by zero. Hence

$$r_0\zeta_0 = \frac{\left\{\frac{6}{h^2}(\psi_2-\psi_0) - r_2\zeta_2\right\}}{\left\{2 + \frac{h\cos\theta}{r_0} - \frac{h^2\cos^2\theta}{4r_0^2}\right\}}. \tag{37}$$

This formula is correct to $O(h^2)$ in ζ and is probably the most convenient and accurate formula that can be used.

As an example of the use of this formula let us consider the Poiseuille flow in a circular pipe. With a pipe radius of twenty units and a centre-line velocity of two units, the stream function and vorticity are given respectively by

$$\psi = 0{\cdot}00125r^4 - r^2$$

and

$$\zeta = 0{\cdot}01r.$$

Suppose that the value of ζ on the boundary ($r = 20$) has to be found from the values of ψ and ζ on the line $r = 19$. In the boundary formula (37) the directed mesh length h is -1 and $\theta = 0$. Substituting in the formula,

$$20\zeta_0 = \frac{6(200 - 198{\cdot}09875) - 19 \times 0{\cdot}19}{(2 - \frac{1}{20} - \frac{1}{1600})} = 4{\cdot}0$$

which gives $\zeta = 0{\cdot}20$ as required by the theory. This complete agreement is to be expected in a Poiseuille flow, because the neglected terms in the derivation of the boundary formula are then zero.

Part II.—The Effects of Viscosity and Orifice Size on a Pitot Tube at Low Reynolds Numbers

Summary. The effects of viscosity and orifice size on a blunt-nosed pitot tube have been theoretically investigated up to a Reynolds number of ten, where the Reynolds number has been based on the radius of the tube. Results are expressed in terms of a pressure coefficient

$$C_p = \frac{p_0 - p_s}{\frac{1}{2}\rho U^2}$$

where p_0 is the pressure measured in the tube, ρ the density of the fluid, and p_s and U the static pressure and velocity in an undisturbed flow at the position of the tube.

The values of C_p for a blunt-nosed tube are found to be less than those for tubes with hemispheroidal heads, but always greater than unity in the range considered. The effect of the orifice size is to decrease C_p as the orifice size increases, this decrease is very small but increases with the Reynolds number. At a Reynolds number of ten the decrease is at most five per cent of the value of C_p when there is no orifice.

It is suggested that the decrease of C_p below unity found in some experimental investigations at a higher Reynolds number could be due to the effects of orifice size.

2.1. *Introduction.* When determining velocities in a fluid from impact pressure measurements with a pitot tube a special interpretation is necessary when the tube Reynolds number is small.

It is usual to assume that the fluid on the stagnation streamline is brought to rest without the action of viscous forces, and that the pressure measured at the tube orifice is the stagnation point pressure. The velocity can then be determined from Bernouilli's equation. When the viscous and inertial forces become comparable in magnitude the Bernouilli formula is inapplicable and a new interpretation is required to determine the velocity correctly.

The geometry of the tube has been found to influence considerably the readings at low Reynolds numbers. The tubes most frequently used are the straight cylindrical blunt-nosed type and those with hemispherical or source shaped heads. The corrections to be applied to the blunt-nosed types at low Reynolds numbers have been found experimentally to be smaller than those required for tubes with hemispheroidal heads. If the tube orifice is large a complex flow pattern is set up inside and around the tube which can so disturb the flow that the pressure recorded is not the true stagnation point pressure; this effect is not confined to measurements at low Reynolds numbers. When the tube orifice is small compared with the tube diameter this flow does not occur to the same extent and the pressure measured differs little from the true stagnation point pressure.

A considerable amount of research has now been done on the effects of viscosity and of probe geometry on pitot tubes, the majority of which has been experimental. The only theoretical bases available for comparison have been either the flow near the stagnation point of a sphere or a prolate spheroid. Reasonable agreement between theory and experiment has been obtained in the cases of hemispherical headed and source shaped tubes. With the blunt-nosed tube we can expect the flow pattern to differ from that around a spheroid and whilst the flow round a spheroid has been used by some authors for comparison the results have not been in agreement and there is little justification for making the comparison.

The earliest work on the effects of viscosity on pitot tubes was that of Miss Barker[11], who experimented with straight cylindrical tubes in a Poiseuille flow. The viscous effects were found

to be appreciable below a Reynolds number of thirty, where the Reynolds number has apparently been based on the internal radius of the tube. Whether the radius was internal or external is not made completely clear when the dimensions of her apparatus are given, but it seems likely that at the mouth of the tube these radii differed only slightly.

Homann[12] has investigated the flow past a sphere by means of boundary-layer theory and also studied the flow experimentally. In terms of a pressure coefficient C_p such that

$$C_p = \frac{p_0 - p_s}{\frac{1}{2}\rho U^2}$$

where p_0 is the pressure measured in the pitot tube, p_s and U the static pressure and the velocity in the undisturbed flow and ρ is the density of the fluid, the result of Homann is given by

$$C_p = 1 + \frac{6}{Re + 0{\cdot}455\sqrt{Re}},$$

where the Reynolds number Re is based on the radius of the sphere. It is difficult to specify the exact range of validity of Homann's theory but it is quite accurate above a Reynolds number of ten. This is supported by the fact that the values of C_p agree quite well with some numerical results given by Jenson[4] for solutions of the complete Navier-Stokes equations for the flow past a sphere at Reynolds numbers up to twenty.

Hurd, Chesky and Shapiro[13] have experimented with cylindrical blunt-nosed tubes and found that between $Re = 60$ and $Re = 1000$ the pressure in the tube is slightly less than in an inviscid fluid, *i.e.*, $C_p < 1$. MacMillan[14] has also experimented with similar tubes and failed to find the decrease of C_p below unity; he did however find it using tubes of rectangular cross section (Ref. 15).

The work of Sherman[16] was carried out in both subsonic and supersonic airstreams using three types of tube, two were source shaped and the other was blunt nosed with a sharp lip. At supersonic speeds a marked tendency for C_p to decrease below unity was found; at subsonic speeds the occurrence of values below unity was slight. Sherman also suggests that the tube Reynolds number should be based on the internal radius of the tube orifice rather than the external radius of the tube. In view of the disturbance caused to the flow at low Reynolds numbers by the tube there seems no reason to assume that the value of C_p is independent of either radius although much closer agreement is obtained between experimental results when the internal radius is used as the characteristic length. Whilst there is considerable scatter in Sherman's results at low Reynolds numbers in subsonic flow, the source shaped tubes tended to give values of C_p following Homann's theory whereas the blunt-nosed tube gave results nearer to those of Miss Barker and the values of C_p were much lower than for the source shaped tubes, the Reynolds number being based on external radius.

The present investigation was conducted with the object of providing a theoretical comparison for use with the blunt-nosed pitot tube, and also to ascertain whether the effect of orifice size could be determined.

2.2. *Theoretical Model.* The model used to arrive at a theoretical solution was as follows: a semi-infinite blunt-ended cylinder with a radius of 1 cm was placed on the axis of a circular pipe of radius 20 cm. Upstream of the cylinder there was a Poiseuille flow and downstream the flow was assumed to tend to that in an annulus. The upstream centre-line velocity was taken as 2 cm/sec. Initially there was no orifice in the cylinder but later the walls were assumed to be infinitely thin so that the orifice effect could be studied. (*See* Figs. 5 and 6.)

The origin of co-ordinates was taken at the stagnation point 0 on the cylinder (*see* Fig. 4) with the z-axis along the axis of the pipe and the r-axis perpendicular to it. We specified $\psi = 0$ on the cylinder surface and $\psi = -200$ on the surface of the containing pipe. The upstream Poiseuille flow was given by

$$\psi = 0{\cdot}00125r^4 - r^2 \tag{1}$$

$$\zeta = 0{\cdot}01r \text{ where } 0 \leqslant r \leqslant 20$$

and the limiting annular flow downstream by

$$\psi = 0{\cdot}0018716r^4 - 1{\cdot}14798r^2 \log r + 0{\cdot}245538r^2 - 0{\cdot}247409 \tag{2}$$

$$\zeta = 0{\cdot}014973r - 0{\cdot}997125/r \text{ where } 1 \leqslant r \leqslant 20.$$

2.3. *The Numerical Solution.* With an initial mesh length of unity, assumed values of ψ and ζ were placed at mesh points throughout the field. Upstream, boundary values given by the Poiseuille flow of Equations (1) were placed about two pipe radii from the cylinder. Downstream, similarly about two pipe radii away, boundary values given by Equations (2) were used. These artificial boundaries were completely arbitrary for it was obvious that the transition from Poiseuille to annular flow could not take place over such a short distance. Placing the boundaries any further away initially would have so increased the size of the field to be worked as to make an attempt at solution impracticable.

Using the methods of Part I, an approximate solution to the Stokes' equations (*i.e.*, the case of zero Reynolds number) was obtained working entirely by hand. The next step in the process was to move the assumed boundaries further away and investigate the effect which this had upon the function values in the neighbourhood in which we were particularly interested. After moving the boundaries further away and settling the field again it soon became apparent that whilst the upstream flow was settling fairly rapidly and the disturbance caused by the insertion of the cylinder was not being propagated very far upstream, the flow downstream could not settle to the annular flow for many pipe diameters. Fortunately this was no serious disadvantage, for changes of quite large magnitude in the function values a short distance downstream were found to have almost no effect on the upstream values. Since our main interest lay in the region around the end of the cylinder and in the upstream flow it was found possible to fix the downstream function values when they were only changing slightly after each recalculation from the finite difference equations, without causing too serious a disturbance of the upstream flow. This procedure was adopted and the field settled. The mesh length was then reduced in the region extending about one pipe radius up and downstream of the stagnation point 0 and further reduced in the region near the cylinder and stagnation point.

At the sharp corner of the cylinder the empirical method introduced by Thom[17] for use in two dimensions was used. In Fig. 7 two values of ζ were used at the point A, one of these was calculated from the values of ψ and ζ at B and used in the recalculation of the function values at B using a diamond, and the other was calculated from the values at C and used in the diamond centred on C for recalculating values there. The two values of ζ at A are artificial, effectively one is on the inner wall of the annulus and the other on the blunt end of the cylinder and both are slightly removed from the actual corner. Repeated subdivision of the field in this neighbourhood has been found to raise these values considerably while hardly affecting the surrounding points.

A sufficiently accurate approximation to the Stokes' flow having been obtained this solution was used to provide a series of starting values for the problem at a finite Reynolds number. The Reynolds number was based on the radius of the cylinder and the upstream centre-line velocity, ν the kinematic viscosity being the parameter used for varying the Reynolds number.

It was found that the flow away from the cylinder at a low Reynolds number deviated only slightly from the solution given by the Stokes' approximation and that changes in the function values at some distance from the cylinder did not affect the solution closer in. This enabled a much smaller field to be used for the finite Reynolds number solutions and the assumption was made that the flow four radii upstream and downstream of the cylinder, and three radii out into the stream, was given by the solution of the Stokes' equations. Initially the field used was even smaller than this and the boundary taken only two radii up and downstream, the extension to four radii still caused only slight changes and it seems that the assumption is reasonably valid provided that it is not used at too high a Reynolds number.

Solutions have been obtained under the assumptions already mentioned at Reynolds numbers of 0, 1·0, 2·5, 5·0 and 10. It was felt that the assumptions made should certainly be valid as far as $Re = 5$ and whilst solutions above this could be obtained care should be taken in interpreting them. The calculations at $Re = 0$ and $Re = 1$ were both initially worked by hand and later checked on an electronic computer; those at $Re = 2{\cdot}5$, $5{\cdot}0$ and 10 were entirely worked on a computer.

When the problem had been solved for a blunt-ended cylinder without an orifice, the geometry was changed to that shown in Fig. 6 where the cylinder is assumed to have infinitesimally thin walls, and the problem reworked. In this case three artificial values of ζ were required at the sharp lip of the cylinder.

2.4. *The Calculation of the Pressure Coefficient.* It was convenient to express the pressure measured at the stagnation point 0 on the cylinder in terms of the coefficient

$$C_p = \frac{p_0 - p_s}{\frac{1}{2}\rho U^2}$$

where p_0 is the pressure measured at 0, p_s the static pressure at 0 in a Poiseuille flow undisturbed by the introduction of the cylinder, ρ the density of the fluid, and U the centre-line velocity in the undisturbed upstream flow.

A point A was taken on the pipe axis at such a distance from 0 that the flow there was practically undisturbed. The pressure coefficient was then given by

$$C_p = \frac{(p_0 - p_A) + (p_A - p_s)}{\frac{1}{2}\rho U^2} = \left(\frac{p_0 - p_A}{\frac{1}{2}\rho U^2}\right)_{\text{Disturbed}} - \left(\frac{p_0 - p_A}{\frac{1}{2}\rho U^2}\right)_{\text{Undisturbed}}.$$

The pressure differences were then determined using Equation (10) of Part I. Between two points β and α on the pipe axis we have

$$\frac{1}{\rho}(p_\alpha - p_\beta) = \frac{q_\beta^2}{2} - \frac{q_\alpha^2}{2} + \nu \int_\alpha^\beta \left(\frac{\partial \zeta}{\partial r} + \frac{\zeta}{r}\right) dz.$$

On the pipe axis both ζ and r are zero, making ζ/r an indeterminate form; L'Hopital's rule gives

$$\frac{\zeta}{r} = \frac{\partial \zeta}{\partial r}.$$

The Reynolds number was based on the radius of the cylinder and the undisturbed centre-line velocity ($U = 2$ cm/sec) whence

$$\nu = \frac{2}{Re}.$$

On substitution the following formula was arrived at for the calculation of C_p:

$$C_p = 1 + \frac{0{\cdot}02l}{Re} - \frac{2}{Re}\int_A^0 \frac{\partial \zeta}{\partial r}\, dz$$

where l is the distance between 0 and A.

2.5. *Results.* Numerical values for ψ and ζ in a portion of the field near to the cylinder at a Reynolds number of five are recorded in Figs. 8 and 9; in Fig. 8 we have the values for the blunt-ended cylinder and in Fig. 9 those for the cylinder with an orifice.

A careful numerical integration led to the values of C_p set out in the Tables below being obtained.

TABLE 1

Blunt-ended Cylinder

Re	C_p
$\to 0$	$\to 2{\cdot}37/Re$
1·0	3·21
2·5	1·818
5·0	1·384
10·0	1·185

TABLE 2

Cylinder with Orifice

Re	C_p
1·0	3·17
2·5	1·765
5·0	1·326
10·0	1·128

The value of C_p in the limiting case $Re \to 0$ is artificial. It should be realised that when we solve the Stokes' approximations by a numerical method the solution is still being obtained for a finite Reynolds number. This Reynolds number varies with position in the field and is related to the order of magnitude of the neglected terms in the finite difference approximations and to the residual at each point in the field.

The variations of pressure and velocity on the stagnation streamline for the blunt-nosed cylinder are shown in Figs. 10 and 11 respectively.

The change of position of the zero streamline with Reynolds number near the cylinder with infinitely thin walls is depicted in Fig. 12. It is seen from Fig. 13 that the streamline enters the tube and that a very weak eddy is set up inside the orifice.

2.6. *Comparison with Experimental Results.* The variation of C_p with Reynolds number, based on the internal radius of the tube, is plotted in Fig. 14. Also shown are the experimental results of Miss Barker, Sherman, Hurd *et al.* and MacMillan for tubes which had a similar geometry to that of the model used in the present investigation. The experimental points are rather scattered but the general agreement with the theoretical result is quite good; also shown is the theoretical result of Homann for the sphere, which lies considerably above the present result.

With the tube Reynolds number based on the external radius the results are given in Fig. 15. Miss Barker's results have been plotted on the assumption that the tube was sharp lipped and the internal and external radii were the same.

MacMillan has drawn faired curves through his own experimental points and also curves through the points of Sherman and Hurd *et al.* with the Reynolds number based on the external diameter of the pitot tube. Plotted on this basis it is apparent that the values of C_p for blunt-nosed tubes lie below those for hemispheroidal headed tubes, and that as the orifice size increases so C_p decreases. The results obtained using the present approach confirm both of these experimental facts. When the internal radius is used in defining the Reynolds number all the experimental results tend to lie much closer together as has been shown by MacMillan. Certainly in the case of the blunt-nosed tube it seems that the internal radius should be used in the definition of the Reynolds number; without further investigation on hemispheroidal headed tubes it is difficult to determine which dimension should be used in their case. The fact that as the orifice size increases so C_p decreases could possibly explain the decrease of C_p below unity as found by Hurd *et al.*, it may be that the orifice effect outweighed the viscous effect around a Reynolds number of 60. Since the orifice and viscous effects are presumably interdependent and have some dependence on the ratio of internal to external radius of the tube, the value of this ratio used by MacMillan may not have been high enough to influence sufficiently the orifice effect in his experiments with circular tubes, and there was no decrease of C_p below unity. The tubes with a rectangular cross section with which MacMillan found $C_p < 1$ had been formed by flattening circular tubes whose original ratio of internal to external radius was between $0{\cdot}8$ and $0{\cdot}9$. If the flattened tubes could be regarded as equivalent to the original circular tubes from which they were formed then this ratio would appear high enough for the orifice effect to outweigh the viscous effect. The tube geometry of Sherman was slightly different and from his results with an open-ended tube there appears to be some Mach number effect even at subsonic speeds. Sherman states that at subsonic speeds there was no tendency for C_p to fall below unity; however, on a close examination of his readings in the range of Reynolds numbers between 50 and 1000 with the open-ended tube, out of some sixty readings about half were either less than or equal to unity. At supersonic speeds C_p was less than unity over a wide range.

This suggestion that C_p decreases below unity at some value of the ratio of internal to external tube radius when the Reynolds number is high enough for the viscous effects to be outweighed by the orifice effect is very tentative. The experimental evidence is by no means conclusive and much scope is still available for further experiment.

Acknowledgement. The author wishes to thank Prof. A. Thom for his valuable help and criticism. Thanks are also due to the Oxford University Computing Laboratory for providing facilities on the Mercury Computer which enabled part of this work to be done.

LIST OF SYMBOLS

r, ϕ, z	Cylindrical polar co-ordinates
ψ	Stokes' stream function
ζ	Vorticity
q_r, q_ϕ, q_z	Components of the velocity
F_r, F_ϕ, F_z	Components of the body force
Δ^2	Operator $\frac{\partial^2}{\partial r^2} + \frac{\partial^2}{\partial z^2}$
E^2	Operator $\frac{\partial^2}{\partial r^2} + \frac{\partial^2}{\partial z^2} - \frac{1}{r}\frac{\partial}{\partial r}$
∇^2	Laplacian operator $\frac{\partial^2}{\partial r^2} + \frac{\partial^2}{\partial z^2} + \frac{1}{r}\frac{\partial}{\partial r}$
ρ	Fluid density
ν	Kinematic viscosity
p_s	Static pressure
p	Pressure
n	Distance between adjacent mesh points
θ	Angle the tangent to $\psi =$ constant makes with the positive direction of the z-axis
(R, Z)	Transformed plane where the r, z axes are rotated through an angle θ
U	Representative velocity
L	Representative length
Re	Reynolds number
C_p	Non-dimensional pressure coefficient

Unprimed symbols are dimensional whereas primed symbols are non-dimensional.

REFERENCES

No.	Author	Title, etc.
1	A. Thom	An investigation of fluid flow in two dimensions. A.R.C. R. & M. 1194. 1929.
2	H. Schlichting	*Boundary Layer Theory.* Pergamon Press. 1955.
3	A. Thom	An arithmetical solution of certain problems in steady viscous flow. A.R.C. R. & M. 1475. 1932.
4	V. G. Jenson	Viscous flow round a sphere at low Reynolds numbers. *Proc. Roy. Soc.* A. 249. 1959. 346.
5	L. Fox	The numerical solution of elliptic differential equations when the boundary conditions involve a derivative. *Phil. Trans. Roy. Soc.* A. 242. 1950.
6	L. C. Woods	A note on the numerical solution of fourth-order differential equations. *Aero. Quart.* V. Pt. 3. September, 1954.
7	A. Thom and C. J. Apelt ..	Note on the convergence of numerical solutions of the Navier-Stokes equations. A.R.C. R. & M. 3061. June, 1956.
8	H. B. Squire	The round laminar jet. *Quart. J. Mech. App. Math.* IV. Pt. 3. 1951.
9	H. L. Agrawal	A new exact solution of the equations of viscous flow with axial symmetry. *Quart. J. Mech. App. Math.* X. Pt. 1. 1957.
10	A. Thom	The arithmetic of field equations. *Aero. Quart.* IV. Pt. 3. August, 1953.
11	M. Barker	On the use of very small pitot tubes for measuring wind velocity. *Proc. Roy. Soc.* A. 101. 1922. 435.
12	F. Homann	The effect of high viscosity on the flow around a cylinder and around a sphere. N.A.C.A. Tech. Memo. 1334. 1952.
13	C. W. Hurd, K. P. Chesky and A. H. Shapiro	Influence of viscous effects on impact tubes. *J. App. Mech.* Vol. 20. No. 2. 1953.
14	F. A. MacMillan	Viscous effects on pitot tubes at low speeds. A.R.C. 16,866. June, 1954.
15	F. A. MacMillan	Viscous effects on flattened pitot tubes at low speeds. A.R.C. 17,106. October, 1954.
16	F. S. Sherman	New experiments on impact pressure interpretation in supersonic and subsonic rarefied air streams. N.A.C.A. Tech. Note. 2995. 1953.
17	A. Thom	Arithmetical solution of equations of the type $\nabla^4\psi$ = constant. A.R.C. R. & M. 1604. 1934.

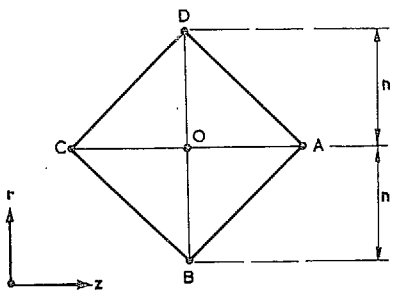

FIG. 1

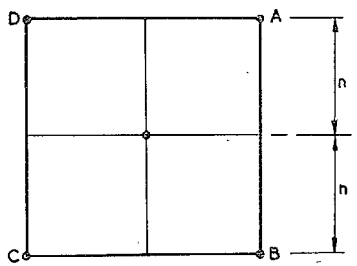

FIG. 2

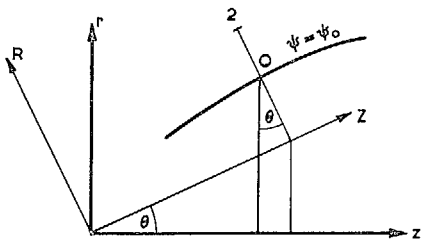

FIG. 3.

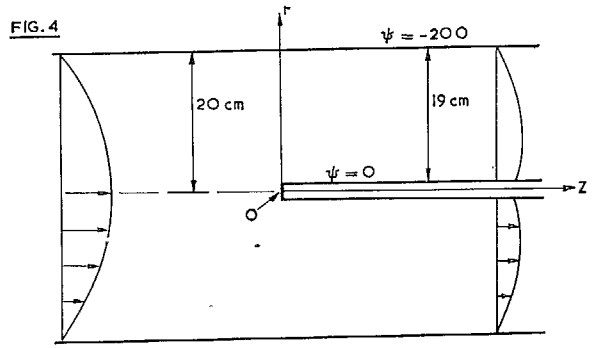

FIG. 4

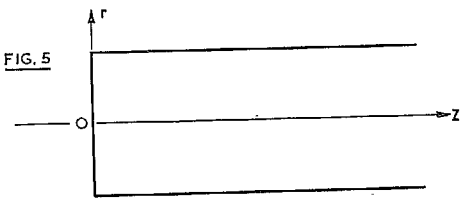

FIG. 5

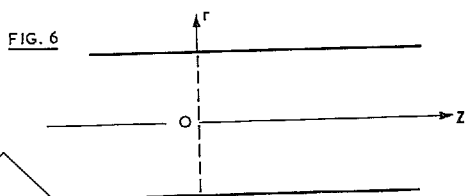

FIG. 6

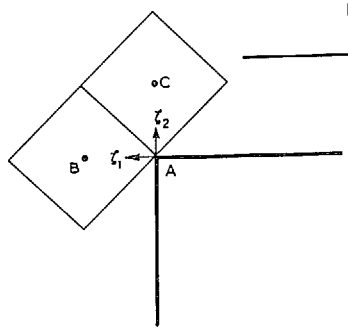

FIG. 7

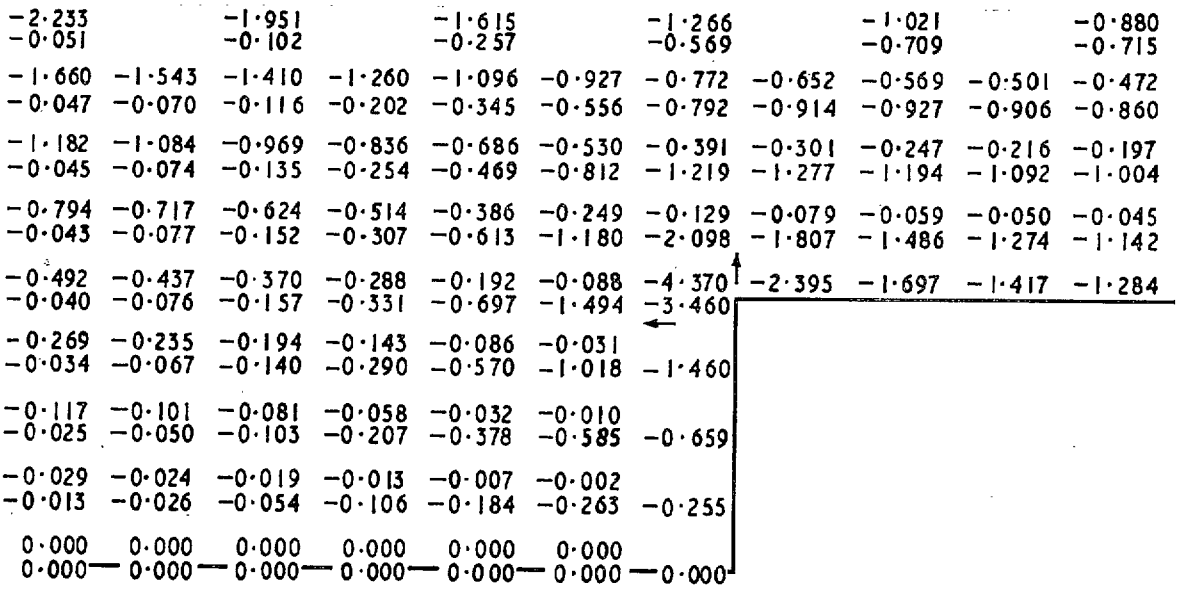

FIG. 8. Flow past pitot tube at $Re = 5$.

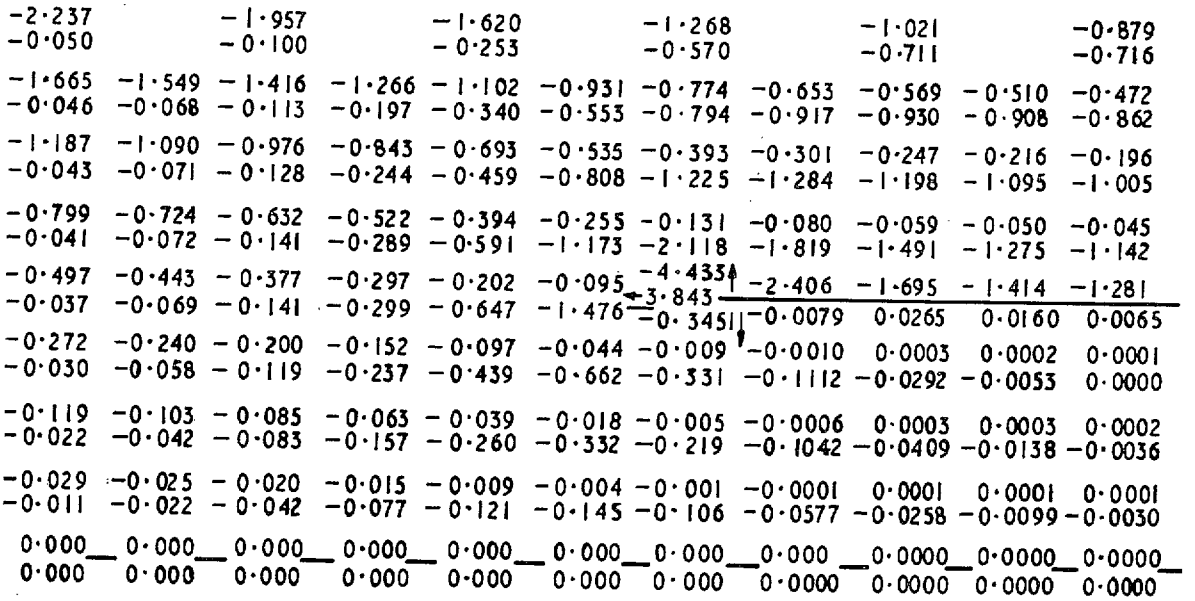

FIG. 9. Flow past open pitot tube at $Re = 5$.

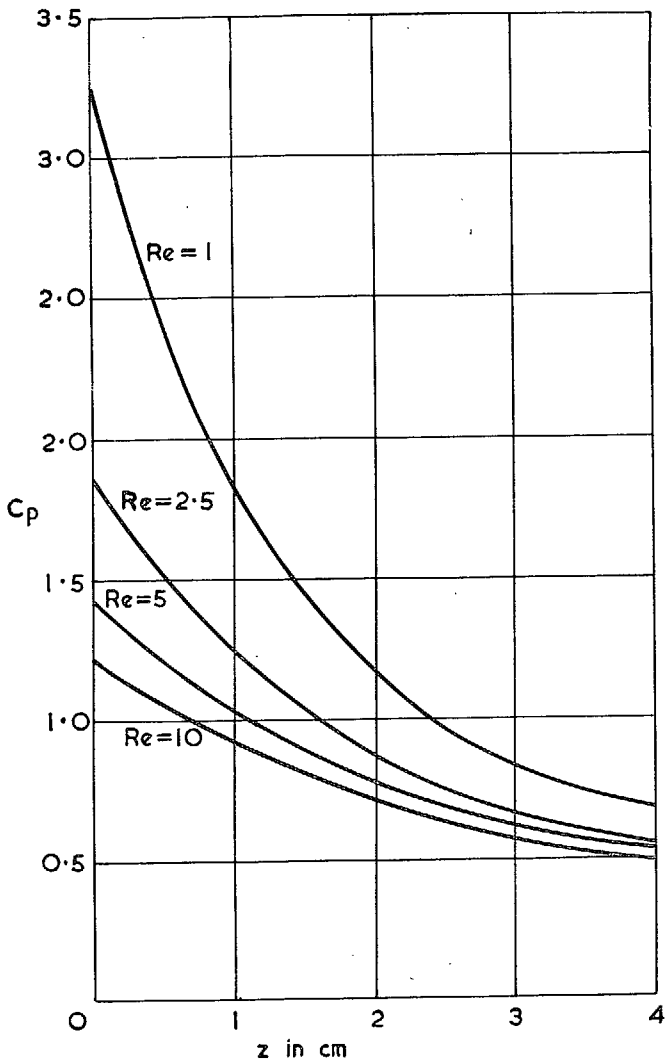

FIG. 10. Pressure variation on stagnation streamline for blunt-ended tube.

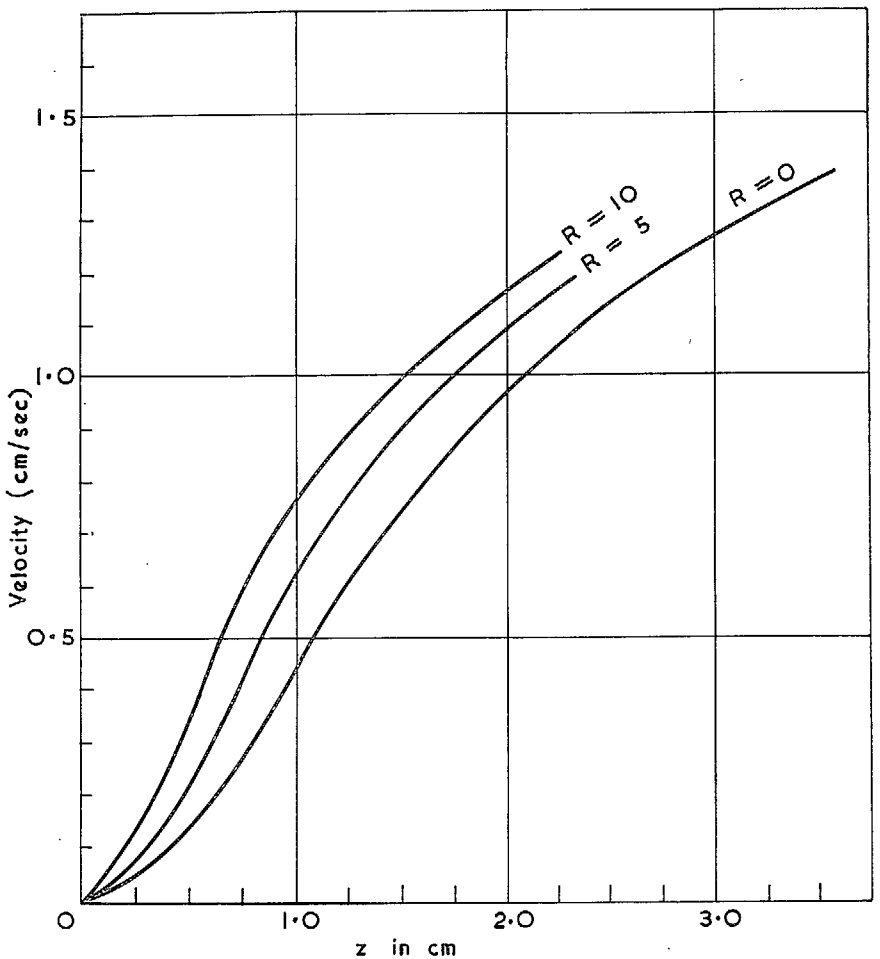

FIG. 11. Velocity variation on stagnation streamline for blunt-ended tube.

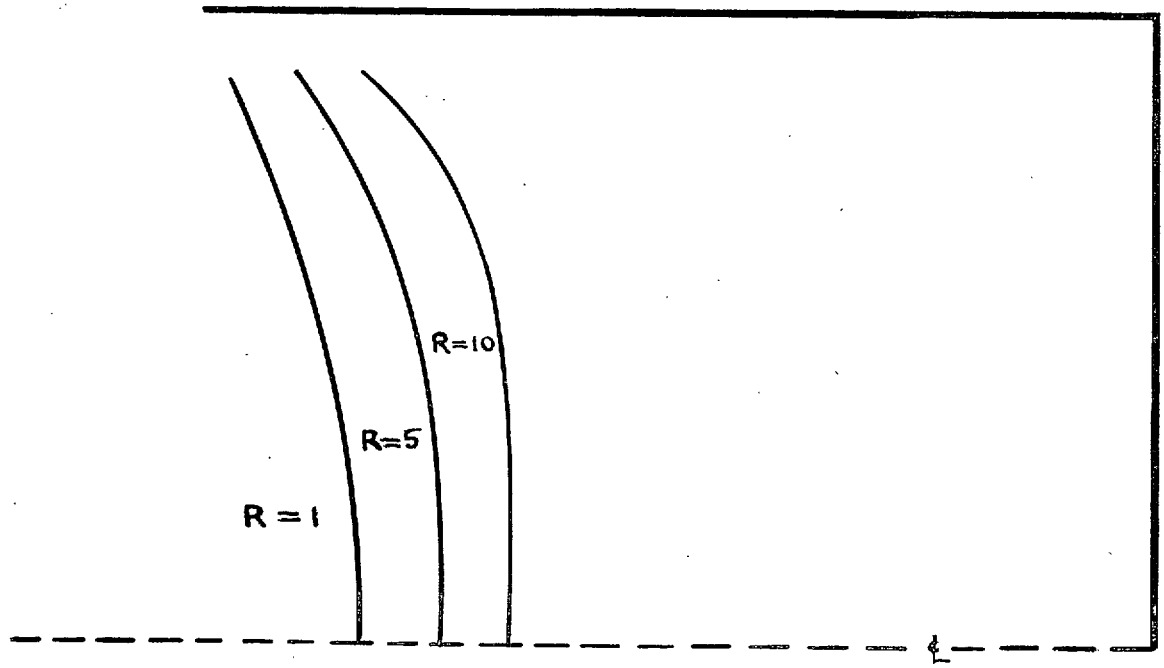

FIG. 12. Position of zero streamlines.

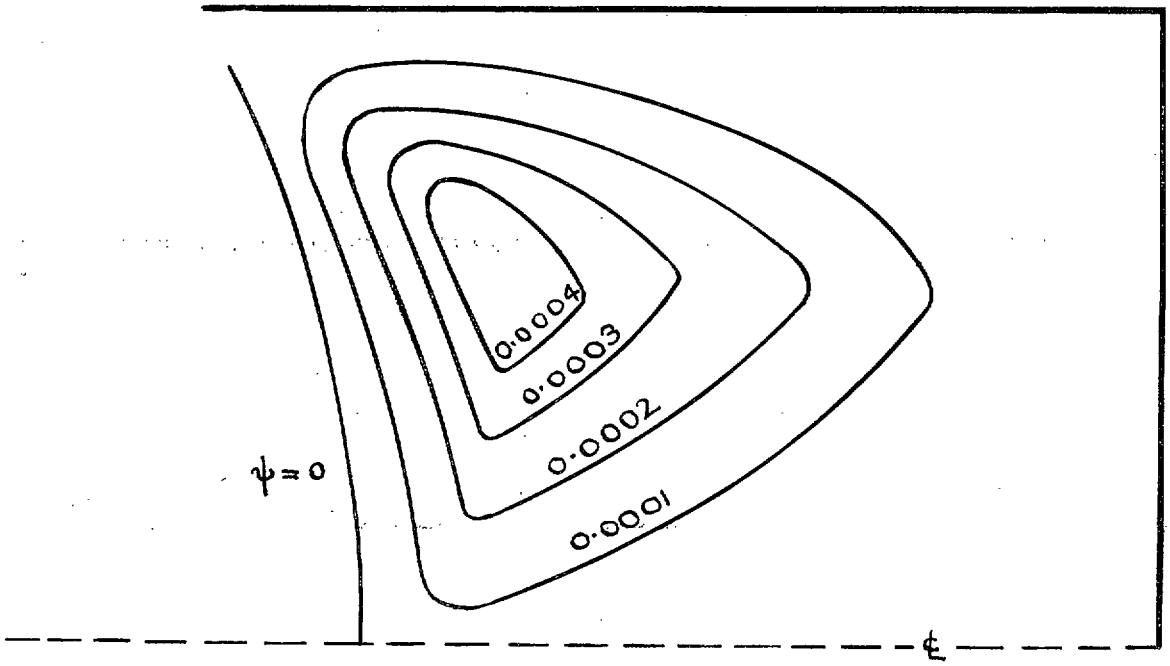

FIG. 13. Flow at $Re = 1$.

(83079) Wt. 67/1876 K.5 12/61 Hw.

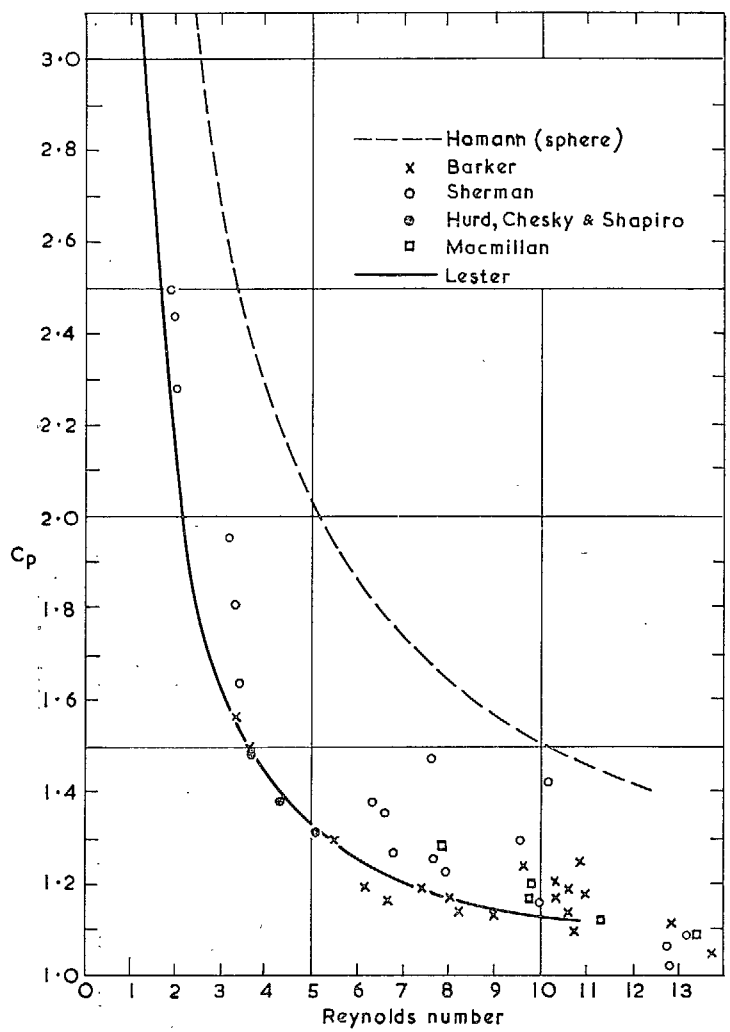

FIG. 14.

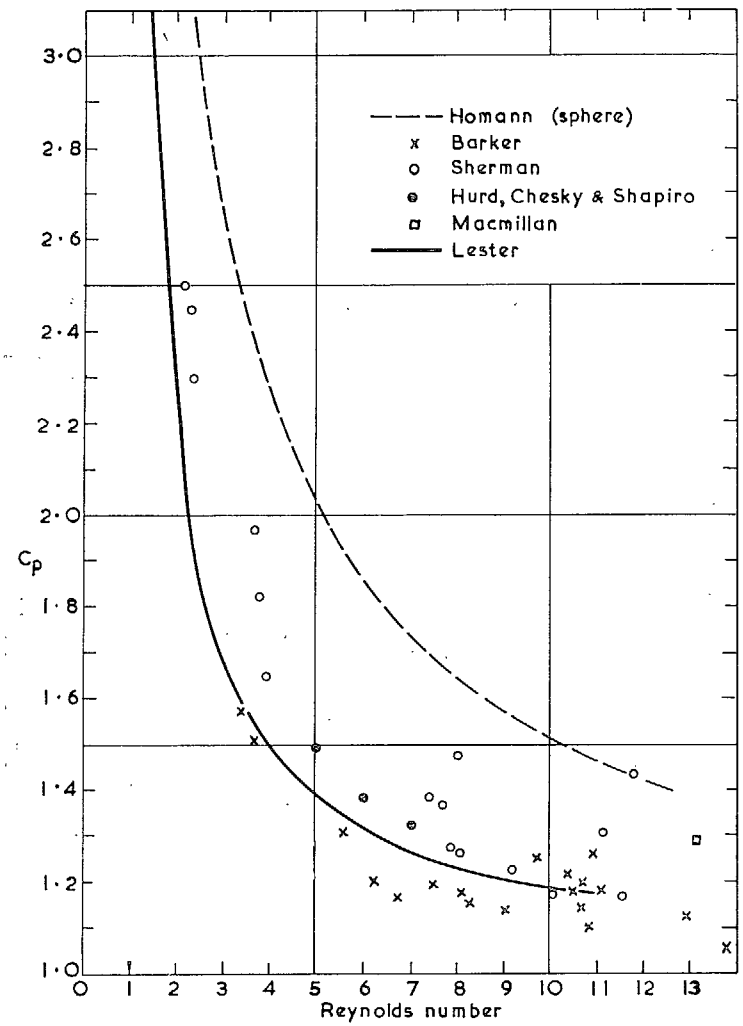

FIG. 15.

Publications of the Aeronautical Research Council

ANNUAL TECHNICAL REPORTS OF THE AERONAUTICAL RESEARCH COUNCIL (BOUND VOLUMES)

1941 Aero and Hydrodynamics, Aerofoils, Airscrews, Engines, Flutter, Stability and Control, Structures. 63*s.* (post 2*s.* 3*d.*)

1942 Vol. I. Aero and Hydrodynamics, Aerofoils, Airscrews, Engines. 75*s.* (post 2*s.* 3*d.*)
Vol. II. Noise, Parachutes, Stability and Control, Structures, Vibration, Wind Tunnels. 47*s.* 6*d.* (post 1*s.* 9*d.*)

1943 Vol. I. Aerodynamics, Aerofoils, Airscrews. 80*s.* (post 2*s.*)
Vol. II. Engines, Flutter, Materials, Parachutes, Performance, Stability and Control, Structures. 90*s.* (post 2*s.* 3*d.*)

1944 Vol. I. Aero and Hydrodynamics, Aerofoils, Aircraft, Airscrews, Controls. 84*s.* (post 2*s.* 6*d.*)
Vol. II. Flutter and Vibration, Materials, Miscellaneous, Navigation, Parachutes, Performance, Plates and Panels, Stability, Structures, Test Equipment, Wind Tunnels. 84*s.* (post 2*s.* 6*d.*)

1945 Vol. I. Aero and Hydrodynamics, Aerofoils. 130*s.* (post 3*s.*)
Vol. II. Aircraft, Airscrews, Controls. 130*s.* (post 3*s.*)
Vol. III. Flutter and Vibration, Instruments, Miscellaneous, Parachutes, Plates and Panels, Propulsion. 130*s.* (post 2*s.* 9*d.*)
Vol. IV. Stability, Structures, Wind Tunnels, Wind Tunnel Technique. 130*s.* (post 2*s.* 9*d.*)

1946 Vol. I. Accidents, Aerodynamics, Aerofoils and Hydrofoils. 168*s.* (post 3*s.* 3*d.*)
Vol. II. Airscrews, Cabin Cooling, Chemical Hazards, Controls, Flames, Flutter, Helicopters, Instruments and Instrumentation, Interference, Jets, Miscellaneous, Parachutes. 168s. (post 2*s.* 9*d.*)
Vol. III. Performance, Propulsion, Seaplanes, Stability, Structures, Wind Tunnels. 168*s.* (post 3*s.*)

1947 Vol. I. Aerodynamics, Aerofoils, Aircraft. 168*s.* (post 3*s.* 3*d.*)
Vol. II. Airscrews and Rotors, Controls, Flutter, Materials, Miscellaneous, Parachutes, Propulsion, Seaplanes, Stability, Structures, Take-off and Landing. 168*s.* (post 3*s.* 3*d.*)

Special Volumes

Vol. I. Aero and Hydrodynamics, Aerofoils, Controls, Flutter, Kites, Parachutes, Performance, Propulsion, Stability. 126*s.* (post 2*s.* 6*d.*)
Vol. II. Aero and Hydrodynamics, Aerofoils, Airscrews, Controls, Flutter, Materials, Miscellaneous, Parachutes, Propulsion, Stability, Structures. 147*s.* (post 2*s.* 6*d.*)
Vol. III. Aero and Hydrodynamics, Aerofoils, Airscrews, Controls, Flutter, Kites, Miscellaneous, Parachutes, Propulsion, Seaplanes, Stability, Structures, Test Equipment. 189*s.* (post 3*s.* 3*d.*)

Reviews of the Aeronautical Research Council

1939–48 3*s.* (post 5*d.*) 1949–54 5*s.* (post 5*d.*)

Index to all Reports and Memoranda published in the Annual Technical Reports

1909–1947 R. & M. 2600 6*s.* (post 2*d.*)

Indexes to the Reports and Memoranda of the Aeronautical Research Council

Between Nos. 2351–2449	R. & M. No. 2450 2*s.* (post 2*d.*)
Between Nos. 2451–2549	R. & M. No. 2550 2*s.* 6*d.* (post 2*d.*)
Between Nos. 2551–2649	R. & M. No. 2650 2*s.* 6*d.* (post 2*d.*)
Between Nos. 2651–2749	R. & M. No. 2750 2*s.* 6*d.* (post 2*d.*)
Between Nos. 2751–2849	R. & M. No. 2850 2*s.* 6*d.* (post 2*d.*)
Between Nos. 2851–2949	R. & M. No. 2950 3*s.* (post 2*d.*)
Between Nos. 2951–3049	R. & M. No. 3050 3*s.* 6*d.* (post 2*d.*)

HER MAJESTY'S STATIONERY OFFICE

from the addresses overleaf

Printed and published by
HER MAJESTY'S STATIONERY OFFICE

To be purchased from
York House, Kingsway, London W.C.2
423 Oxford Street, London W.1
13A Castle Street, Edinburgh 2
109 St. Mary Street, Cardiff
39 King Street, Manchester 2
50 Fairfax Street, Bristol 1
35 Smallbrook, Ringway, Birmingham 5
80 Chichester Street, Belfast 1
or through any bookseller

Printed in England

S.O. Code No. 23-3240